



HAL
open science

Titan's ionosphere: A survey of solar EUV influences

O. Shebanits, E. Vigren, J. -E. Wahlund, M. K. G. Holmberg, M. Morooka,
N. J. T. Edberg, K. E. Mandt, J. H. Waite

► **To cite this version:**

O. Shebanits, E. Vigren, J. -E. Wahlund, M. K. G. Holmberg, M. Morooka, et al.. Titan's ionosphere: A survey of solar EUV influences. *Journal of Geophysical Research Space Physics*, 2017, 122, pp.7491-7503. 10.1002/2017JA023987 . insu-03676978

HAL Id: insu-03676978

<https://insu.hal.science/insu-03676978>

Submitted on 24 May 2022

HAL is a multi-disciplinary open access archive for the deposit and dissemination of scientific research documents, whether they are published or not. The documents may come from teaching and research institutions in France or abroad, or from public or private research centers.

L'archive ouverte pluridisciplinaire **HAL**, est destinée au dépôt et à la diffusion de documents scientifiques de niveau recherche, publiés ou non, émanant des établissements d'enseignement et de recherche français ou étrangers, des laboratoires publics ou privés.

Copyright

RESEARCH ARTICLE

10.1002/2017JA023987

Key Points:

- Ion and dust grain charge densities near the ionospheric peak enhanced while the peak altitudes are decreased by higher solar EUV flux
- Ionospheric nightside charge densities decrease with higher solar EUV flux
- Chapman theory not applicable for Titan's (dayside) ionosphere below 1200 km altitude

Correspondence to:

O. Shebanits,
oleg.shebanits@ifru.se

Citation:

Shebanits, O., E. Vigrén, J.-E. Wahlund, M. K. G. Holmberg, M. Morooka, N. J. T. Edberg, K. E. Mandt, and J. H. Waite (2017), Titan's ionosphere: A survey of solar EUV influences, *J. Geophys. Res. Space Physics*, 122, 7491–7503, doi:10.1002/2017JA023987.





Received 6 FEB 2017

Accepted 16 JUN 2017

Accepted article online 21 JUN 2017

Published online 3 JUL 2017

Titan's ionosphere: A survey of solar EUV influences

O. Shebanits^{1,2} , E. Vigrén¹, J.-E. Wahlund¹ , M. K. G. Holmberg^{3,4}, M. Morooka¹, N. J. T. Edberg¹ , K. E. Mandt^{5,6}, and J. H. Waite^{5,6} 

¹Swedish Institute of Space Physics, Uppsala, Sweden, ²Department of Physics and Astronomy, Uppsala University, Uppsala, Sweden, ³Université de Toulouse, UPS-OMP, IRAP, Toulouse, France, ⁴CNRS, IRAP, Toulouse, France, ⁵Department of Physics and Astronomy, University of Texas at San Antonio, San Antonio, Texas, USA, ⁶Space Science and Engineering Division, Southwest Research Institute, San Antonio, Texas, USA

Abstract Effects of solar EUV on positive ions and heavy negative charge carriers (molecular ions, aerosol, and/or dust) in Titan's ionosphere are studied over the course of almost 12 years, including 78 flybys below 1400 km altitude between TA (October 2004) and T120 (June 2016). The Radio and Plasma Wave Science/Langmuir Probe-measured ion charge densities (normalized by the solar zenith angle) show statistically significant variations with respect to the solar EUV flux. Dayside charge densities increase by a factor of ≈ 2 from solar minimum to maximum, while nightside charge densities are found to anticorrelate with the EUV flux and decrease by a factor of ≈ 3 –4. The overall EUV dependence of the ion charge densities suggest inapplicability of the idealized Chapman theory below 1200 km in Titan's ionosphere. Nightside charge densities are also found to vary along Titan's orbit, with higher values in the sunward magnetosphere of Saturn compared to the magnetotail.

Plain Language Summary Saturn's moon Titan hosts a fully developed atmosphere of nitrogen and methane extending up to almost an entire Titan radius above the surface. The top atmosphere is ionized primarily by the solar radiation on the dayside and energetic particles on the nightside, initiating a complex organic chemistry. Effects of solar radiation on Titan's ionosphere are studied over the course of almost 12 years, (October 2004 to June 2016). The dayside ionospheric plasma densities (ions and charged dust grains) cannot be described by the Chapman theory. On the nightside, the plasma densities anticorrelate with the solar radiation flux, possibly due to photochemistry of the upper atmosphere being altered by the higher flux. Nightside plasma densities are also found to vary along Titan's orbit, with higher values in the sunward magnetosphere of Saturn compared to the magnetotail.

1. Introduction

Titan, the largest moon of Saturn (2575 km radius), hosts a fully developed, N₂- and CH₄-dominated atmosphere extending to almost a whole radius above its surface [Niemann *et al.*, 2005; Wahlund, 2005; Edberg *et al.*, 2010; Galand *et al.*, 2014, and references therein]. On the dayside, the atmosphere is ionized primarily by the solar extreme ultraviolet (EUV) radiation with peak ionization at ≈ 1100 km altitude [Cravens *et al.*, 2006; Ågren *et al.*, 2009; Shebanits *et al.*, 2013; Vigrén *et al.*, 2014]. On the nightside, at altitudes below 1200 km (also on the dayside but deeper down), the main ionization source is the flux of energetic particles from the Kronian magnetosphere [Ågren *et al.*, 2007; Cravens *et al.*, 2008, 2009] (a cartoon of Titan's ionospheric plasma profiles is shown in Figure 1). The ionization balance is regulated by different mechanisms, in particular, by transport [Müller-Wodarg *et al.*, 2008; Crary *et al.*, 2009; Cui *et al.*, 2010], ion-electron dissociative recombination, and ion-ion mutual neutralization [e.g., Vigrén *et al.*, 2015]; their respective relative contributions vary with altitude.

In the deepest ionosphere (880–1000 km altitude), the in situ observations by the Cassini spacecraft (S/C) have revealed negatively charged ions/dust particles (~ 5 nm) [Coates *et al.*, 2007], with abundances comparable to or higher than the free electrons [Ågren *et al.*, 2012; Shebanits *et al.*, 2013, 2016]. In this region, the number density of the positive ions [singly charged, Thissen *et al.*, 2011] is enhanced due to the (comparatively low) ion production rate being compensated by a slow chemical loss rate [Lavvas *et al.*, 2013; Vigrén *et al.*, 2014; Shebanits *et al.*, 2016]. The ionization sources initiate a complex ion chemistry (see, e.g., Vuitton *et al.* [2014], and references therein, modeled following the observations of heavy positive and negative ions at the lower altitudes reported in Coates *et al.* [2007, 2009], Crary *et al.* [2009], Wahlund *et al.* [2009], Shebanits *et al.* [2013], and Wellbrock *et al.* [2013]), ultimately producing a dusty

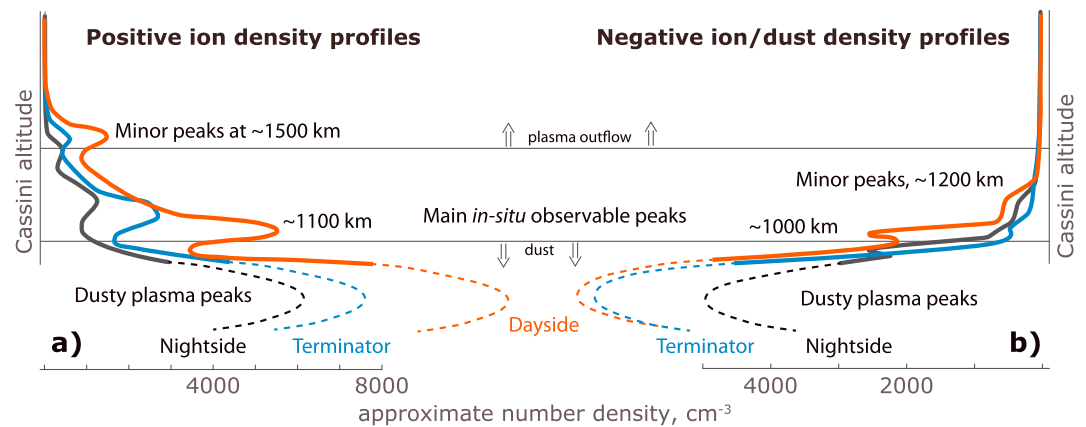


Figure 1. Schematic representation of plasma density profiles in Titan’s ionosphere on the dayside (orange), terminator (blue), and nightside (black). The dusty plasma peaks are below the lowest altitude reached by the Cassini S/C. Based on average ion density profiles from the RPWS/LP measurements.

plasma that is characterized by a significant electron depletion [Shebanits et al., 2016] and aerosols further down [Lavvas et al., 2013].

The ionizing solar EUV flux evidently plays a key role in the complex organic chemistry of Titan’s dayside ionosphere as the main source of energy. Recent research revealed the influence of the solar cycle on Titan’s ionosphere, showing that electron [Edberg et al., 2013] and positive ion number densities for lighter species (<100 amu) [Madanian et al., 2016] are enhanced during the solar maximum, including the ions not directly produced by the ionizing EUV flux. Moreover, Sagnières et al. [2015] showed that the ion number densities correlate with the local ionization rate, although the correlation is significantly stronger for the short-lived ions than for the long-lived ones. The nightside may be affected by the solar EUV indirectly due to possible (but not verified) day-to-night transport mechanisms [Cui et al., 2010] and EUV-dependent variations in Saturn’s magnetospheric corotational plasma flow.

In this study we use in situ measurements by the Radio and Plasma Wave Science (RPWS) Langmuir probe (LP) on board the Cassini S/C to investigate the effects of the varying solar EUV flux on the ion population, adding the heavier positive ions and the negative ions/dust grains to the picture. Section 2 gives a description of the instruments and data processing. The results are presented and discussed in section 3. The conclusions are summarized in section 4.

2. Instruments and Analysis Method

2.1. Instruments

The Langmuir Probe (LP) is part of the Radio and Plasma Wave Science (RPWS) instrument package. It collects plasma current as a function of bias voltage, from which plasma densities, temperatures, and speeds may be derived as well as the S/C potential [Wahlund, 2005; Ågren et al., 2009]. In Titan’s ionosphere the probe performs double voltage sweeps between ±4 V (except for TA and TB) in 1024 steps (+4 V to −4 V and back to +4 V), collecting electron current for positive bias voltages and ion current for negative bias voltages. For the purpose of this study we use the charge densities for positive ions and negative charge carriers (ions and dust grains) derived from the ion part of the sweep, a derivation that relies on the S/C potential extracted from the electron part of the sweep and the mean ion mass measurements by the Ion and Neutral Mass Spectrometer (INMS) instrument as described in Shebanits et al. [2016].

The solar EUV data are translated to Saturn in distance and time (phase) from the solar irradiance measurements (daily average at 1 AU) by the Solar EUV Experiment (SEE) instrument from the Thermosphere Ionosphere Mesosphere Energetics and Dynamics (TIMED) mission and the Solar Stellar Irradiance Comparison Experiment (SOLSTICE) from the Solar Radiation and Climate Experiment (SORCE) mission (<http://lasp.colorado.edu/lisird/>). The TIMED/SEE measurements are used to obtain the total ionizing flux for Titan’s ionosphere, and combined TIMED/SEE and SORCE/SOLSTICE measurements are used for cross-referencing the translation to Saturn. All the EUV measurements in this study therefore refer to the

unattenuated solar EUV flux just outside Titan's ionosphere (i.e., atmospheric extinction not applied). The translation in time (phase) achieves $\approx 600''$ accuracy for the orbital position of Saturn due to the ephemeris prediction algorithm utilizing a two-body model. This precision is sufficient for the purposes of this study, as explained below.

2.2. Solar EUV and the Photoelectron Current

The ionization limit for the dominant species (N_2), is 79.6 nm [Schunk and Nagy, 2009]. To obtain the total ionizing flux F_{EUV} , we therefore integrate the TIMED/SEE solar EUV irradiance spectrum between 0.5 and 79.5 nm. The translation to Saturn can be checked by comparing the photoelectron current (I_{pe}) measured by the RPWS/LP and a theoretical I'_{pe} derived with the solar EUV irradiance. For this purpose, the SORCE/SOLSTICE spectrum replaces the TIMED/SEE for wavelengths > 115 nm due to the recent TIMED/SEE detector degradation for wavelengths > 120 nm (<http://lasp.colorado.edu/lisird/>). To the best of our knowledge, no photoelectric yield measurements have been carried out for a TiN surface at the time of this study. The "next best" yield function from Brace *et al.* [1988] is used instead; the authors used it for a molybdenum- and rhenium-coated LP, although it is based on an average of the laboratory measurements of several metals, e.g., tungsten, gold, aluminum, and stainless steel. This metal average yield function has artificial cut-offs at wavelengths ≤ 20 nm and ≥ 160 nm due to their relatively small contributions ($< 3\%$) to the total I_{pe} . Nevertheless, it gives a sufficient approximation for the TiN-coated RPWS/LP together with the measured solar EUV irradiance up to 160.5 nm, as explained below.

The measured photoelectron current I_{pe} is usually removed in the analysis, it is also negligible compared to the ion current (\propto density) below 1200 km in Titan's ionosphere due to the atmospheric EUV extinction. However, the current collected in the thinnest plasma of Saturn's magnetosphere is dominated by the I_{pe} . To extract it, the RPWS/LP data set is filtered by removing data from Saturn's shadow, the equatorial plane crossings (± 2 days), all the targeted flybys of Saturn's moons (± 1 h), and all the data within $9 R_S$ of Saturn (R_S is the Saturn radius, $\approx 60,000$ km). Additionally, a S/C attitude correction is applied to eliminate the contributions of the TiN-coated stub that the RPWS/LP is mounted on [Jacobsen *et al.*, 2009], by the method described in Holmberg *et al.* [2012].

The resulting photoelectron current is plotted in Figure 2a as a function of time. The first part (marked FIT 1) shows the unperturbed "original" current, from the arrival at Saturn in mid-2004, which is used for the correction of the subsequent current shifts. The second part (FIT 2) is a shift due to a possible influence of the magnetospheric sheet flapping during 2006; removing equatorial crossings does not work as a filter for this period but the net effect is trivially corrected for by assuming a constant sheet ion density (and therefore the ion current to the probe), on average. The third part (FIT 3) is the current before the major shift during at least nine consecutive passages through Saturn's radiation belts in 2008 (exact number is difficult to identify due to the dynamics of Saturn's magnetosphere), which caused a degradation of the RPWS/LP electronics. The net effect is a shift of all the measured current by a constant value (< 0.2 nA), which is corrected for in the analysis. The last part (FIT 4) is the current after the radiation belt passages. The correction of the photoelectron current is performed by fitting it to the theoretical current I'_{pe} , derived with the photoelectron yield function Y from Brace *et al.* [1988] and the solar EUV flux up to 160.5 nm (Figure 2b) as $I'_{pe} = \int_{\lambda} Y F_{EUV} d\lambda$. The slope of the "original" current (red) is used to fit the subsequent current shifts because the photoelectric properties of the coating are assumed to be constant—the probe is regularly cleaned by setting it to a large negative bias voltage and sputtering the surface with high-energy ions for longer time periods in Saturn's magnetosphere. It is not recommended to use the solar EUV flux for such a correction directly because the photoelectric yield function depends on the wavelength and each wavelength varies differently during the solar cycle; this effect is prominent in the deviation of the I'_{pe} (Figure 2a, blue line) from the solar EUV flux (Figure 2a, gray line) of 2014–2015, compared to the similar EUV levels of 2004–2005. Comparing the corrected I_{pe} (Figure 2c, black line) and the theoretical I'_{pe} (blue line) shows that the difference (dashed line) is below the RPWS/LP noise level of 0.1 nA [Gurnett *et al.*, 2004], validating both the yield function approximation and the negligibility of the magnetospheric ion current. This control also demonstrates that the I_{pe} measured by the RPWS/LP (and generally, an S/C-mounted Langmuir probe in similar plasma conditions as shown by Brace *et al.* [1988]) can be used as a local empirical approximation of the solar EUV flux (gray line), including the small-scale variations.

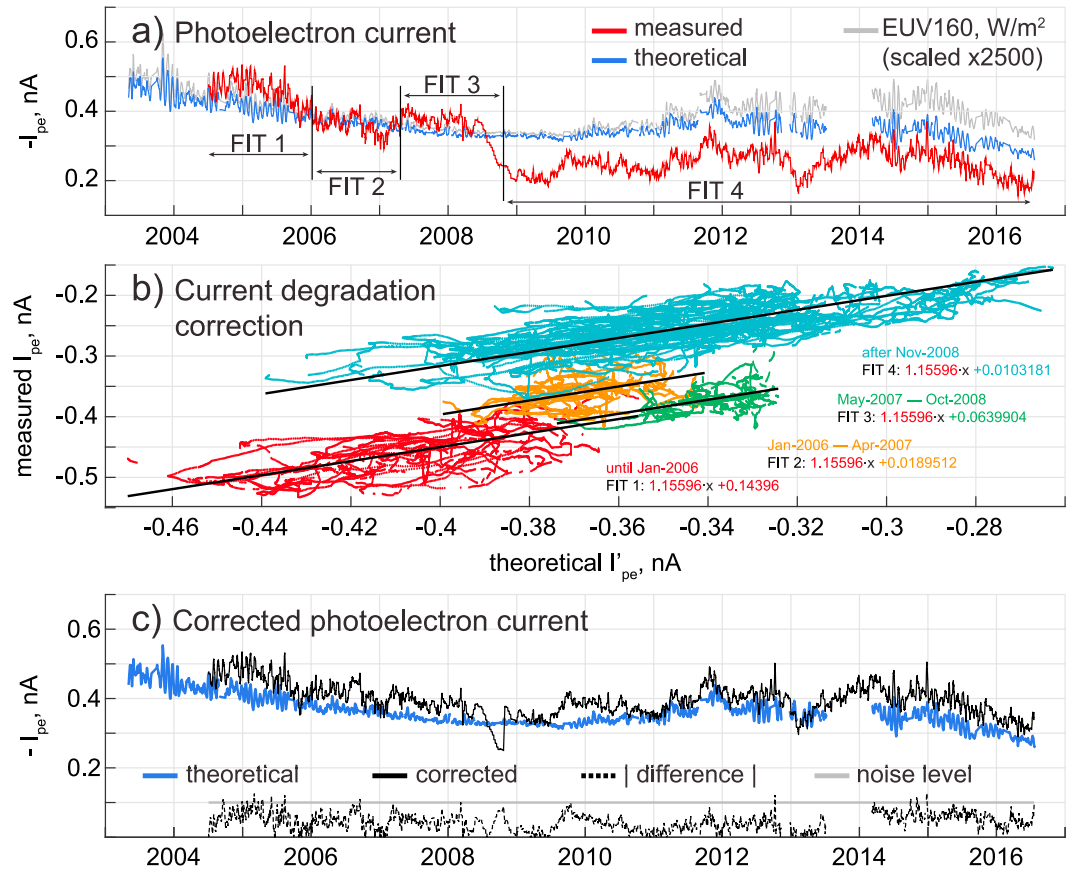


Figure 2. (a) Comparison of the measured (red) and theoretical (blue) photoelectron current, I_{pe} . The integrated solar EUV flux <160 nm is plotted in gray for reference. (b) Measured I_{pe} plotted versus the theoretical I'_{pe} derived with the integrated solar EUV flux (<160 nm) and the yield function from *Brace et al.* [1988] (Flux \times Yield, integrated over wavelength). Best linear fits are plotted as solid black lines. Orange part of the measured current is separated due to a possible influence of the magnetospheric sheet flapping (across the orbit of the Cassini S/C) during 2006. (c) The corrected I_{pe} (black) versus the theoretical I'_{pe} (blue); the difference between these currents is plotted as a dashed black line. The RPWS/LP noise level is shown as a gray line at 0.1 nA for reference.

2.3. Data Reduction

The RPWS/LP derived charge densities of the positive ions and negative ions and dust grains are sorted into two sets each: peak densities below 1200 km (solar EUV and magnetospheric particle ionization peaks [see, e.g., *Cravens et al.*, 2008; *Ágren et al.*, 2009; *Galand et al.*, 2010; *Shebanits et al.*, 2013]) and closest approach (CA) maxima at altitudes 950–1050 km (see section 3). The latter imply that there is at least one peak below the CA altitude and are used as representative densities for the deepest ionosphere reachable by the Cassini S/C, populated by heavier ions and dust grains [*Wahlund et al.*, 2009; *Wellbrock et al.*, 2013; *Shebanits et al.*, 2016]. The upper limit of 1200 km altitude is imposed to remove the possible influences of the ion outflows [*Cui et al.*, 2010] and the ion drift effects in the upper ionosphere (collisionless, ≥ 1400 km) [*Rosenqvist et al.*, 2009]. Examples of altitude profiles and the high- and low-altitude peaks of the measured charge densities are shown in Figure 3.

After sorting, the data sets are processed following the method described in *Edberg et al.* [2013]. The first step is to detrend by the solar zenith angle (SZA) using a cosine function:

$$n_{\pm} = a \cdot \cos(b \cdot SZA), \tag{1}$$

where n_{\pm} is the charge density at dayside/terminator ($SZA < 110^\circ$) and a and b are fit parameters. To avoid the trend contamination by the EUV-enhanced charge densities, only the solar minimum n_{\pm} is used here (a subset of flybys with the solar EUV flux below $35 \mu W m^{-2}$). It should be noted that fitting the same function to the solar maximum values does not change the b parameter beyond its error margin, and the largest effect

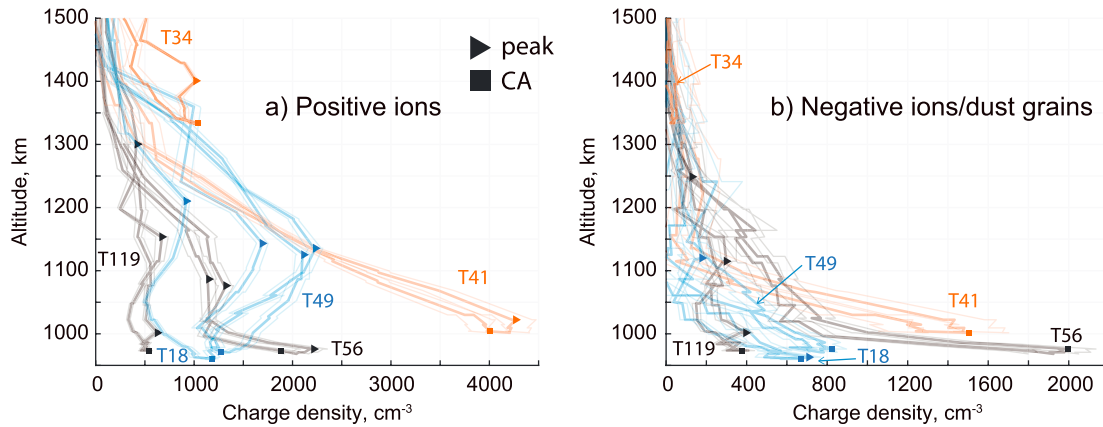


Figure 3. Examples of high- and low-altitude charge densities of (a) positive ions and (b) negative ions/dust grains from flybys T18, T34, T41, T49, T56, and T119. Dayside flybys are colored in orange, terminator in blue, and nightside in black; the triangles mark the peaks and the squares mark the closest-approach (CA) maxima.

of this on the n_{\pm} values is for small SZA ($<20^{\circ}$), where we have nearly no data points (see section 3 below). Regarding the fitting function, the idealized theoretical description of the SZA variation requires a $\sqrt{\cos}$ dependency [Chapman, 1931], but the exact expression assumes an isothermal plane-stratified atmosphere of single-ion species absorbing a monochromatic radiation flux and no chemistry, all of which are not applicable to the altitudes of interest. Using a simple cosine function instead, we receive an empirical fit to the data which is more than sufficient for the purpose of the trend removal. For the nightside ionosphere, the charge densities are normalized by a median value instead. There is a statistically significant variation with respect to the Saturn Local Time (SLT), in agreement with the enhancements caused by the flux of energetic particles from the tail magnetosphere [Mitchell et al., 2009; Westlake et al., 2011], the trend is weak, however, and has very little impact on the consequent analysis. It should also be noted that removing the SLT trend does not account for the fluctuations of the high-energy particle precipitation (e.g., by an equivalent of auroral processes on Titan). The SZA and SLT trends are shown in section 3. After this step the charge densities in the dayside, terminator, and nightside ionosphere are fitted to the solar EUV flux (if there is a statistically significant correlation) using a power law:

$$n'_{\pm} \propto F_{\text{EUV}}^k, \tag{2}$$

where F_{EUV} is the solar EUV flux $<80 \text{ nm}$, n'_{\pm} is the charge density detrended by the SZA (plus for the positive ions and minus for the negative ions/dust grains), and k is a fit parameter with the theoretical expectation value of 0.5 [Chapman, 1931]. Dayside (SZA $< 70^{\circ}$), terminator (SZA 70° – 110°), and nightside (SZA $> 110^{\circ}$) regions of the ionosphere are investigated separately due to different conditions in these regions, while both the dayside and terminator regions are ionized mainly by the solar EUV (the terminator ionospheric peaks are $\sim 100 \text{ km}$ higher in altitude due to the extent of Titan’s ionosphere). The nightside region is ionized mainly by Saturn’s magnetospheric electrons, protons, and oxygen ions [Cravens et al., 2008; Galand et al., 2014, Figure 11.25, and references therein].

It should be noted that detrending by the EUV fit propagates very large errors (power law coefficients), and an investigation of further underlying variations is not possible with the current data set. This includes potential seasonal, latitudinal, and longitudinal variations, for instance.

3. Results and Discussion

The RPWS/LP-derived data set is shown in Figure 4 and includes flybys from TA to T120. A first thing to note is that there are typically two peaks during low solar activity. A minor peak (lighter ions) at altitudes $\geq 1200 \text{ km}$ ($n_{+} = 300 - 1800 \text{ cm}^{-3}$, $n_{-} = 200 - 500 \text{ cm}^{-3}$) is due to transport and inflow of magnetospheric particles [Ågren et al., 2007; Cravens et al., 2009]. A major peak (heavier ions and dust grains) below $\leq 1200 \text{ km}$ ($n_{+} \leq 7500 \text{ cm}^{-3}$, $n_{-} = 500 - 4000 \text{ cm}^{-3}$, “main peak” in Figure 1, see also examples in Figure 3) is due to the solar EUV ionization on the dayside and the inflow of magnetospheric particles on the nightside. The minor peaks are typically below 1000 cm^{-3} and $\approx 100 \text{ km}$ wide, whereas the major peaks span $\approx 400 \text{ km}$

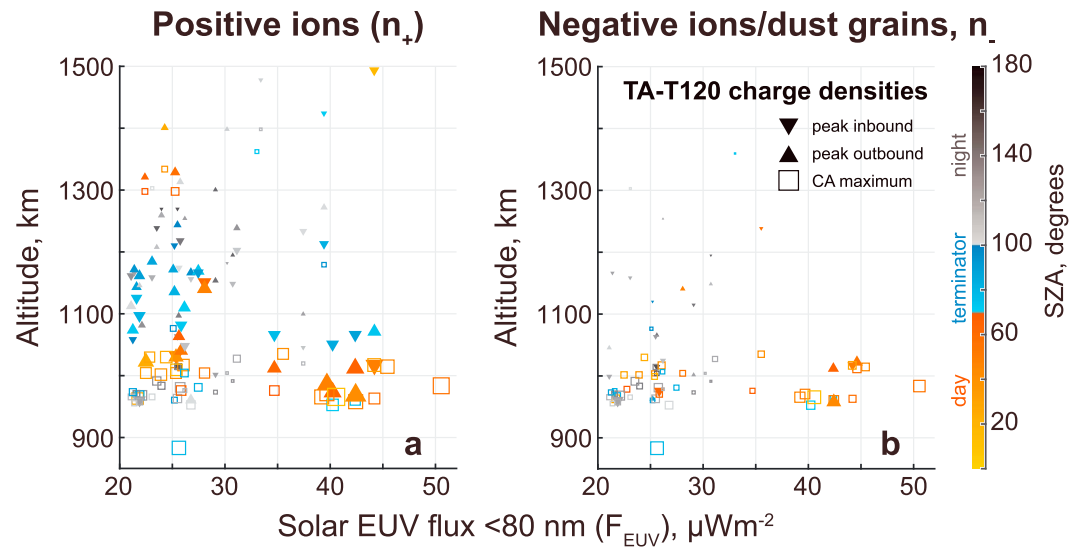


Figure 4. The RPWS/LP data set of (a) positive ion and (b) negative ion/dust grain charge densities from TA to T120 flybys plotted in altitude versus the solar EUV flux (integrated up to 80 nm). The triangles represent the peak charge densities for the inbound (down triangles) and the outbound (up triangles) part of the Cassini trajectory, the squares represent the CA maximum charge density for the cases where the peak altitude was not reached. The colors represent the SZA variation, orange gradient for the dayside, blue for the terminator, and gray for the nightside ionosphere. Marker size is proportional to the charge density.

and reach $\approx 4000 \text{ cm}^{-3}$. During high solar activity the higher altitude peaks seemingly vanish, possibly because they become indistinguishable in the overall EUV-enhanced density profiles. Plotting the positive ion charge densities (Figure 4a) versus the solar EUV flux (F_{EUV}) and the SZA (color coded) reveals the strongest trends: the SZA dependence, with higher n_+ (larger markers) in the dayside ionosphere [see also Ågren *et al.*, 2009; Shebanits *et al.*, 2013; Madanian *et al.*, 2016] and the EUV dependence in the dayside (orange) and terminator (blue) ionosphere, with higher n_+ at higher F_{EUV} , while the peak (triangles) altitudes decrease. This effect was also reported for the calculated production rates of N_2^+ and the observed densities of the primary ion species by Madanian *et al.* [2016]. The negative ion/dust grain charge densities (n_-) also increase with increasing F_{EUV} (Figure 4b) although with increasing dayside peak altitudes: for the lower values of F_{EUV} the peaks are below the CA altitudes of $\approx 1000 \text{ km}$ (as indicated by the empty squares marking the CA maximum n_-), but for the higher F_{EUV} values the peaks (triangles) begin to appear above the CA altitudes. The apparent increase in the negative ion/dust grain peak altitude may be an effect of the solar EUV interrupting the formation of the heavier negative ions/dust grains (more details below)—the lighter species, which peak at higher altitudes [Wellbrock *et al.*, 2013], would then become dominant and effectively shift the total peaks to higher altitudes.

Strictly speaking, the y coordinate of the triangles in Figure 4 correspond to altitudes along individual Cassini trajectories. The SZA varies during each flyby and it is not guaranteed that these values reflect the location of density maxima along the vertical direction. The location of the maxima may be close to the maxima of the ion-electron pair production rate (P_e) but can also be shifted downward by an increased fraction of negative ions with decreasing altitude [Vigren *et al.*, 2014; Shebanits *et al.*, 2016]. In any case, we consider that estimates of P_e along the dayside Titan flybys are needed for an interpretation of the presented trend of decreasing (increasing) altitude of the positive (negative) ion number density peaks with increasing EUV flux. We are therefore planning another study to evaluate P_e along the Cassini trajectory using a similar approach as Vigren *et al.* [2013] but on an extended set of flybys. This requires the number density profiles of N_2 (and possibly CH_4), which are assessable from the INMS measurements.

3.1. Charge Density Normalization

To isolate the impact of the solar cycle, the dayside and terminator ($\text{SZA} < 110^\circ$) charge densities are first detrended by the SZA (divided by their respective fits in Figures 5a and 5b). The nightside ($\text{SZA} > 110^\circ$)

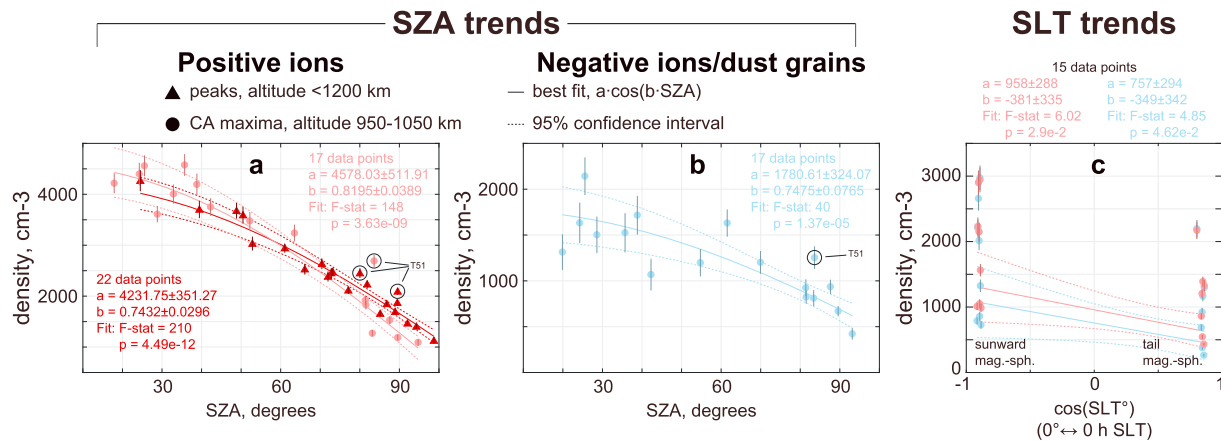


Figure 5. SZA plots of the charge densities of (a) positive ion peaks (bright red) and CA maxima (faint red) and (b) negative ion/dust grain CA maxima (faint blue) during solar minimum. SZA limit for the fit is 100°. (c) Nightside charge densities plotted versus SLT. Peak values are at altitudes <1200 km, CA maxima are at altitudes 950–1050 km. Error bars show 95% confidence intervals for each measurement (2σ). Best (statistically significant) fits used for detrending are plotted as solid lines and dashed lines show their respective 95% confidence intervals (2σ).

charge densities are normalized by the median instead. The positive ion peak and CA maximum densities exhibit very similar SZA trends (Figure 5a), despite covering different mass and altitude ranges. One should also keep in mind that the RPWS/LP does not discriminate between the ion masses in the collected current [see, e.g., Shebanits et al., 2016]. We therefore simply conclude that the current data set does not show any significant SZA-dependent differences for the positive ions between the mass groups populating the altitudes of <1200 km (peaks) and 950–1050 km (CA maxima). There is a (weak) dependency on the SLT (Figure 5c), with low F statistic and large uncertainties, despite the fit passing the significance threshold of p value < 0.05 (note that the SLT has been converted into degrees with 0° corresponding to 0 h SLT). The SLT trends for the CA maxima of the heavier positive ions and negative ions/dust grains are also similar. These similarities of the SZA and SLT trends across positive/negative ions and different altitude ranges may reflect characteristics of a dusty plasma, wherein negative ions account for a significant part of the negatively charged population, and where electron attachment to complex neutrals not only yields enhanced negative ion densities but also enhances the lifetime of the positive ions [Vigren et al., 2014; Shebanits et al., 2016]. The main ionization source in Titan’s nightside ionosphere is the flux of Kronian magnetospheric particles, which was found to vary with Titan’s position in Saturn’s magnetosphere [Mitchell et al., 2009], in particular, an enhancement of the ring current intensity in the tail and further increase toward sunward magnetosphere. The SLT-trends in Figure 5c show a matching asymmetry: a statistically significant difference in the charge density maxima, with higher values when Titan is in the sunward magnetosphere compared to the magnetotail. This variation is also consistent with enhanced N_2 densities during higher magnetospheric particle flux as discussed in Westlake et al. [2011]. The peak densities show no statistically significant SLT variation, and we interpret this as an effect of the altitude difference between the peaks (≈ 1000 – 1200 km) and the maxima (950–1050 km, see Figure 4) since the magnetospheric particles are deposited primarily in the lower ionosphere [Cravens et al., 2008; Galand et al., 2014, Figure 11.25, and references therein].

3.2. Solar Cycle Dependencies

The EUV dependencies are clearly seen when plotting the detrended charge densities versus the solar EUV flux (Figure 6). For the n_- peaks on the dayside/terminator there are not enough data points and the fit could not be performed; on the nightside (Figure 6f) the fit does not pass the significance criteria (F test with p value < 0.05), but it is consistent with the corresponding fit of the positive ions (Figure 6e). The CA maxima of the positive ion and negative ion/dust grain charge densities at the terminator (Figures 6c and 6d) also fall a bit short on the F test. Remarkably, the data points with the largest fit residuals are all from the T51 flyby, which has enhanced charge densities (compared to the overall profile) as illustrated in Figure 5. Removing T51 from the data set improves the EUV fits enough to pass the significance test (Figure 7, the positive ion peaks are also refitted for consistency). For the dayside and nightside, the peak charge densities and the CA maxima

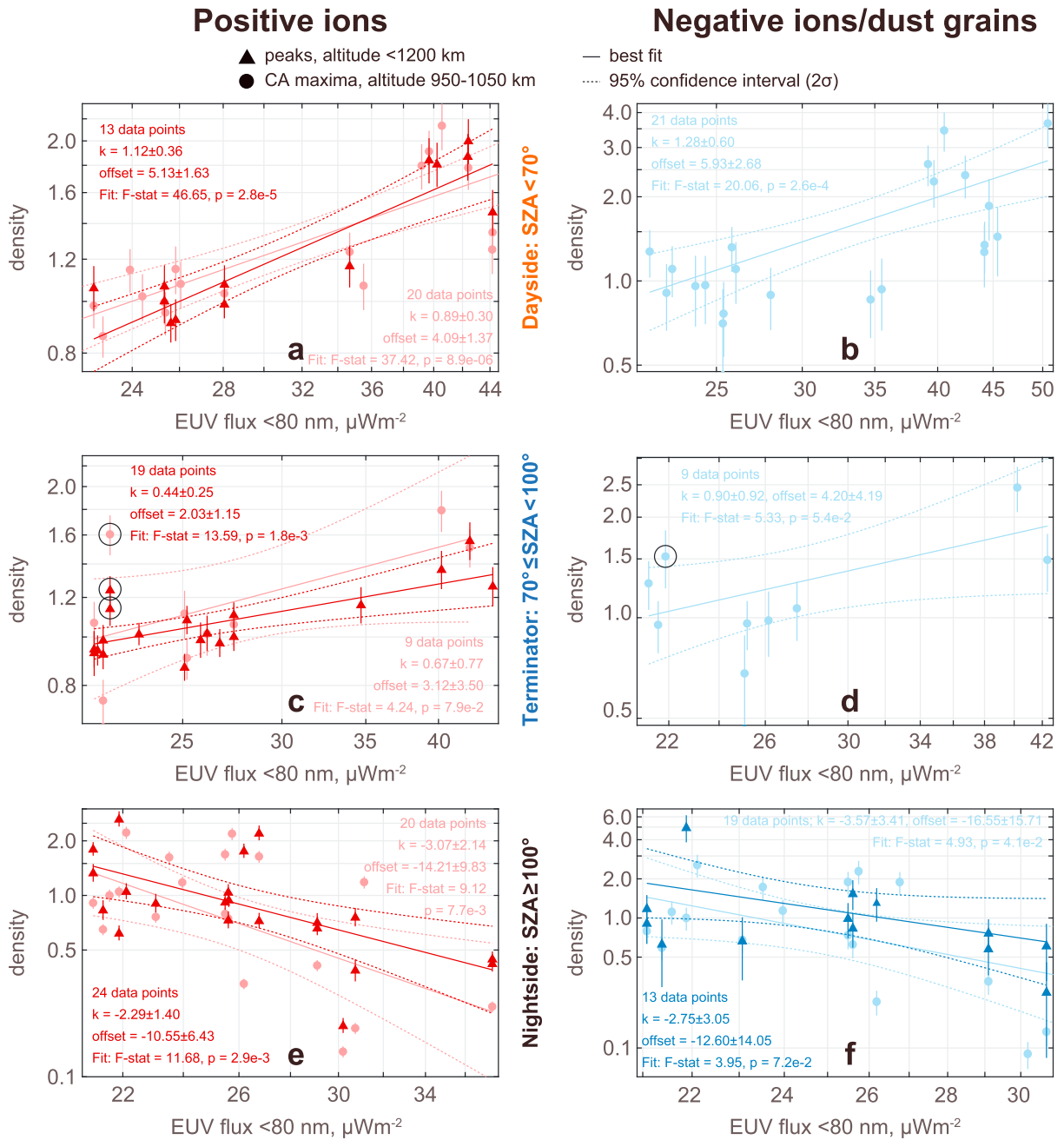


Figure 6. SZA-detrended peaks (black triangles) and maxima (black circles) of (a, c, and e) positive ion charge density and (b, d, and f) negative ion/dust grain charge density, SZA-detrended on the dayside (Figures 6a and 6b) and terminator (Figures 6c and 6d) and normalized by the median on the nightside (Figures 6e and 6f) ionosphere. Best fits are plotted as solid lines and the corresponding confidence intervals as dashed. Note the log scale on all axis. The coefficient k in the legend is from equation (2) and offset is a proportionality factor, i.e., $\log_{10} n_{\pm} = k \log_{10} F_{EUV} + \text{offset}$. All error bars and confidence intervals are 95% confidence (2 σ). The data points marked by black circles are from T51.

of the positive ions have very similar EUV trends, i.e., no significant differences are detected with the presented data set. It should also be noted that the nightside EUV trends are clear both with the median normalization and SLT detrending, although the error margins are much greater in the latter case. Interestingly, both peak and max n_+ and n_- correlate with F_{EUV} on the dayside, a factor ≈ 2 ($\approx 4000 \text{ cm}^{-3}$) increases between minimum and maximum solar activity (similar enhancements have also been observed by the Cassini INMS for positive ions <100 amu [Madanian et al., 2016]). At the same time, the charge densities strongly anticorrelate with F_{EUV} on the nightside of Titan, a factor $\approx 3-4$ ($\approx 3000-4000 \text{ cm}^{-3}$)

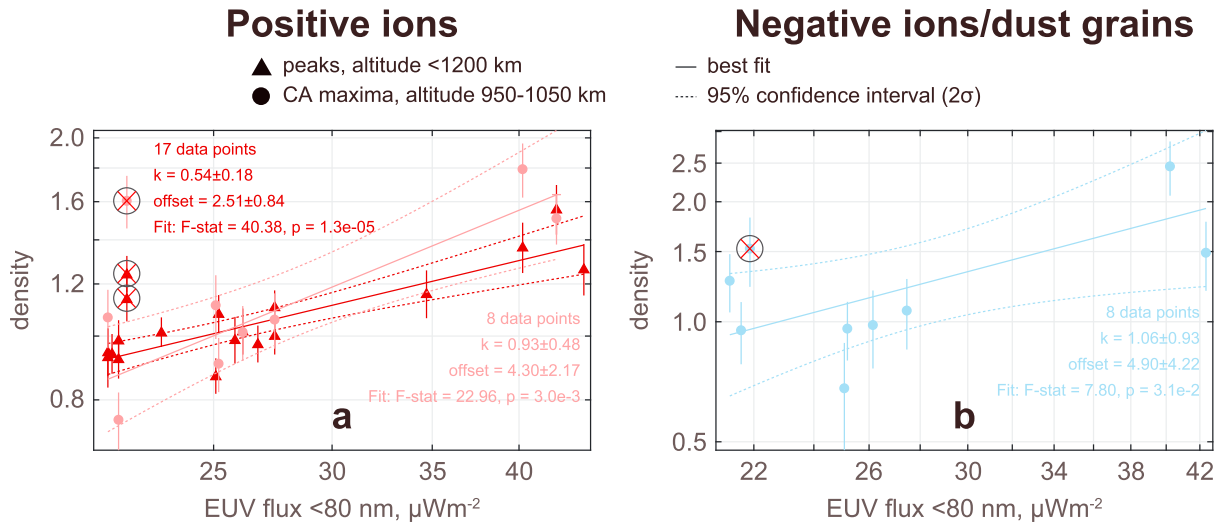


Figure 7. Same as (Figures 6c and 6d) but without the T51 points (crossed-out).

decrease (Figures 6d and 6e; fit coefficients are summarized in Table 1), and despite the fact that there are no measurements of nightside for high F_{EUV} ($\geq 40 \mu W m^{-2}$, see Figures 6d and 6e) that cover the altitudes <1200 km, the trends of both n_+ and n_- are consistent (as expected due to the coupled ion-ion reactions [Shebanits et al., 2016]).

As mentioned above, the Chapman theory [Chapman, 1931] assumes an isothermal, plane-stratified atmosphere consisting of a single ion species that absorb a flux of a single wavelength, none of which are

Table 1. Summary of the Fit Statistics and Coefficients With 95% Confidence Intervals for the Variations in the Charge Densities^a

	Positive Ions				Negative Ions			
	Peaks, $\begin{bmatrix} a_1 \\ a_2 \end{bmatrix}$	# Obs F Stat P Value	CA, $\begin{bmatrix} a_1 \\ a_2 \end{bmatrix}$	# Obs F Stat P Value	Peaks, $\begin{bmatrix} a_1 \\ a_2 \end{bmatrix}$	# Obs F Stat P Value	CA, $\begin{bmatrix} a_1 \\ a_2 \end{bmatrix}$	# Obs F Stat P Value
<i>Ionization at solar min (EUV < 35 $\mu W m^{-2}$), $a_1 \cdot \cos(a_2 \cdot SZA)$ or $a_1 + a_2 \cdot \cos(SLT^\circ)$</i>								
SZA trend	4231.75 ± 351.27	22	4578.03 ± 511.91	17	X	4	1780.61 ± 324.07	17
	0.7432 ± 0.0296	n/a	0.819 ± 0.0389	n/a		n/a	0.7475 ± 0.0765	n/a
		n/a		n/a		n/a		n/a
SLT trend	X	14	958 ± 288	15	X	9	757 ± 294	15
		n/a	-381 ± 335	6.02		n/a	-349 ± 342	4.85
		n/a		$2.9e-2$		n/a		$4.62e-2$
<i>Detrending by EUV, $\log_{10} n_{\pm} = a_1 \log_{10} F_{EUV} + a_2$,</i>								
SZA < 70°	1.12 ± 0.36	13	0.89 ± 0.30	20	X	6	1.28 ± 0.60	21
	5.13 ± 1.63	46.65	4.09 ± 1.37	37.42		n/a	5.93 ± 2.68	20.06
		$2.8e-5$		$8.9e-6$		n/a		$2.6e-4$
70° ≤ SZA < 100°	0.44 ± 0.25	19	0.67 ± 0.77	9	X	2	0.90 ± 0.92	9
	2.03 ± 1.15	13.59	3.12 ± 3.50	4.24		n/a	4.20 ± 4.19	5.33
		$1.8e-3$		$7.9e-2$		n/a		$5.4e-2$
70° ≤ SZA < 100° without T51	0.54 ± 0.18	17	0.93 ± 0.48	8	X	2	1.06 ± 0.93	8
	2.51 ± 0.84	40.38	4.30 ± 2.17	22.96		n/a	4.90 ± 4.22	7.80
		$1.3e-5$		$3.0e-3$		n/a		$3.1e-2$
SZA ≥ 100°	-2.29 ± 1.40	24	-3.07 ± 2.14	20	-2.75 ± 3.05	13	-3.57 ± 3.41	19
	10.55 ± 6.43	11.68	-14.21 ± 9.83	9.12	12.60 ± 14.05	3.95	-16.55 ± 15.71	4.93
		$2.9e-3$		$7.7e-3$		$7.2e-2$		$4.1e-2$

^aMissing coefficients: insufficient number of points and absence of a significant variation are marked with "X." SZA and SLT are in degrees in all of the equations.

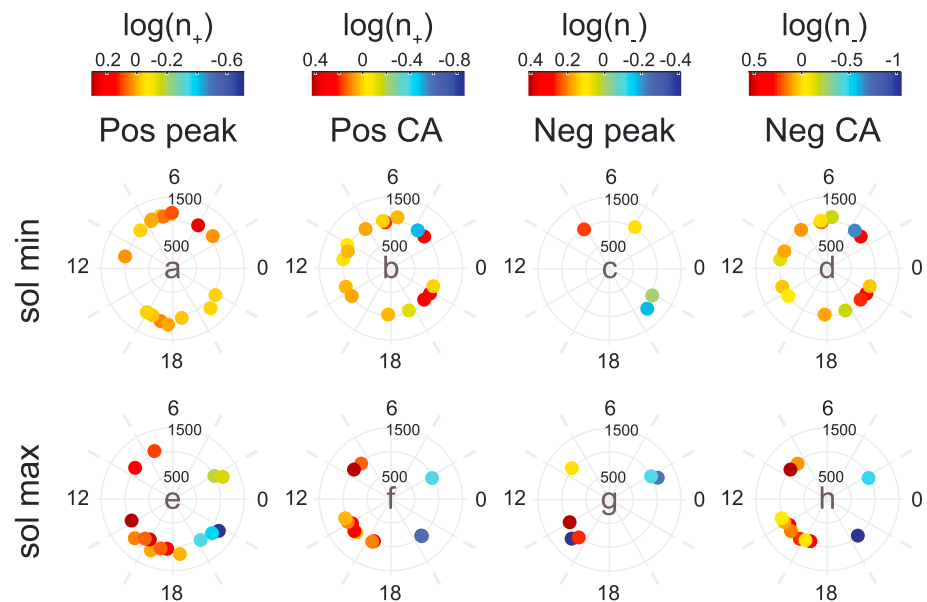


Figure 8. Titan Local Time (LT) plots of the detrended charge densities (by SZA on the dayside and by median on the night-side) from Figure 6. The radial axis is altitude in kilometers. Data points close to the polar regions (within 30° from the ecliptic normal) have been removed due to approximately constant illumination at the altitudes of interest. The EUV boundary between the minimum and maximum in this plot is shifted to $26.5 \mu\text{W m}^{-2}$ to equalize the amount of data points.

applicable in Titan’s ionosphere (subjected to a variable EUV flux) below 1200 km altitude. Despite this, the electron density peaks have been found to be proportional to the square root of the ionizing flux [Edberg et al., 2013]. The positive ion and negative ion/dust grain charge densities, however, exhibit a statistically significant trend with the power law coefficients (Figures 6a and 6b; Table 1) that deviate from the theoretical value of 0.5 by 1 σ at altitudes <1200 km and by 2 σ at altitudes <1050 km on the dayside. The closest value is $k=0.44 \pm 0.25$ for the positive ion peaks at the terminator (Figure 6c, for n_- there are not enough data points for a statistically significant trend), but this is interpreted as a transition from the dayside to the night-side. Therefore, the presented analysis strongly implies that the Chapman theory is not applicable to ions and dust grains in Titan’s ionosphere below 1200 km altitude.

3.3. Nightside Conundrum

As evident from Figure 6, not only are the nightside charge densities *not* oblivious to F_{EUV} but *decrease* with the increasing flux, strongly indicating that any horizontal transport below 1200 km altitude must be much slower than the chemistry—if the transport was faster one would expect to see similar EUV dependencies across the entire ionosphere. Indeed, using empirical and model estimates of the horizontal ion winds, $\sim 230 \text{ m/s}$ [Müller-Wodarg et al., 2008; Cray et al., 2009] at $\sim 1000 \text{ km}$ altitude, puts the time needed to transport ions from the noon ionosphere to midnight to $\sim 13.5 \text{ h}$, while the average lifetime of the heavy ions is estimated to $\sim 2 \text{ h}$ using the presented SZA-detrended charge densities and an ion-ion neutralization rate coefficient of $\sim 10^{-7} \text{ cm}^3 \text{ s}^{-1}$ [Vigren et al., 2014]. Plotting the SZA-detrended densities (normalized by the median on the nightside) in Titan Local Time (LT) for solar minimum and maximum (Figure 8) shows the same EUV trends as in Figure 6 and suggests a local production of (a large part of) the nightside ions as the charge densities change abruptly across the dusk region of the ionosphere, $\approx 8 \text{ h}$ (the positive ion peak densities seem to carry over; however, these are the densities used for the normalization).

A case of chemistry dominating over the day-to-night transport is an equivalent of an ionosphere consisting primarily of short-lived ions. Such a scenario would not have any correlation with the EUV flux on the night-side (sketched in Figure 9a). On the other hand, a composition of primarily long-lived ions would homogenize the EUV-dependencies in the same way as dominating transport (or superrotation, Figure 9b). A mix of both short- and long-lived ions would result in a positive correlation both on the dayside and on the nightside, Figure 9c. A possible explanation is that the solar EUV changes the photochemistry of the dayside upper atmosphere which results in the observation of less ions on the nightside (sketched in Figure 9d). For

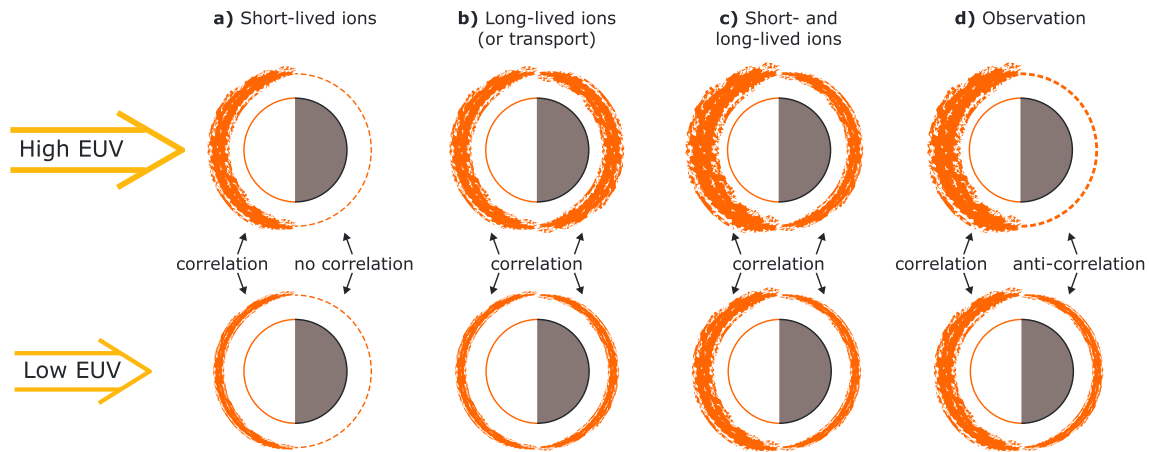


Figure 9. Different scenarios for the dayside and nightside plasma density (orange) variations due to solar EUV: ionosphere populated primarily by (a) short-lived ions, (b) by long-lived ions, and (c) by a mix of both, contrasted (d) by the observed case. Note that transport (e.g., superrotation) has the same effect as the long-lived ions (Figure 9b). Thicker lines correspond to higher plasma densities.

example, a higher EUV may enhance the dayside electron densities and the frequency of the photodissociation, the former would speed up the dissociative recombination, terminating the production chains of heavy complex organic molecules (charged or neutral), while the latter eradicates those already formed. In such a case, with a reduced number of heavy molecules, there would be more free electrons (less attachment sites, i.e., less negative ions) to recombine with the positive ions, pulling the positive ion densities down. However, this is a speculation and detailed modeling is needed for verification since the presented data set incorporates all but the last two flybys of Titan by the Cassini S/C and will not be much extended until the next mission to Titan. This makes it impossible to check the local time variation over the nightside ionosphere alone, for instance, as evident from Figure 8, the nightside has very poor flyby coverage during the solar maximum, although it does look like the nightside charge densities increase from ≈ 20 h to ≈ 3 h LT (Figures 8e–8h), there are simply not enough points to draw a definite conclusion.

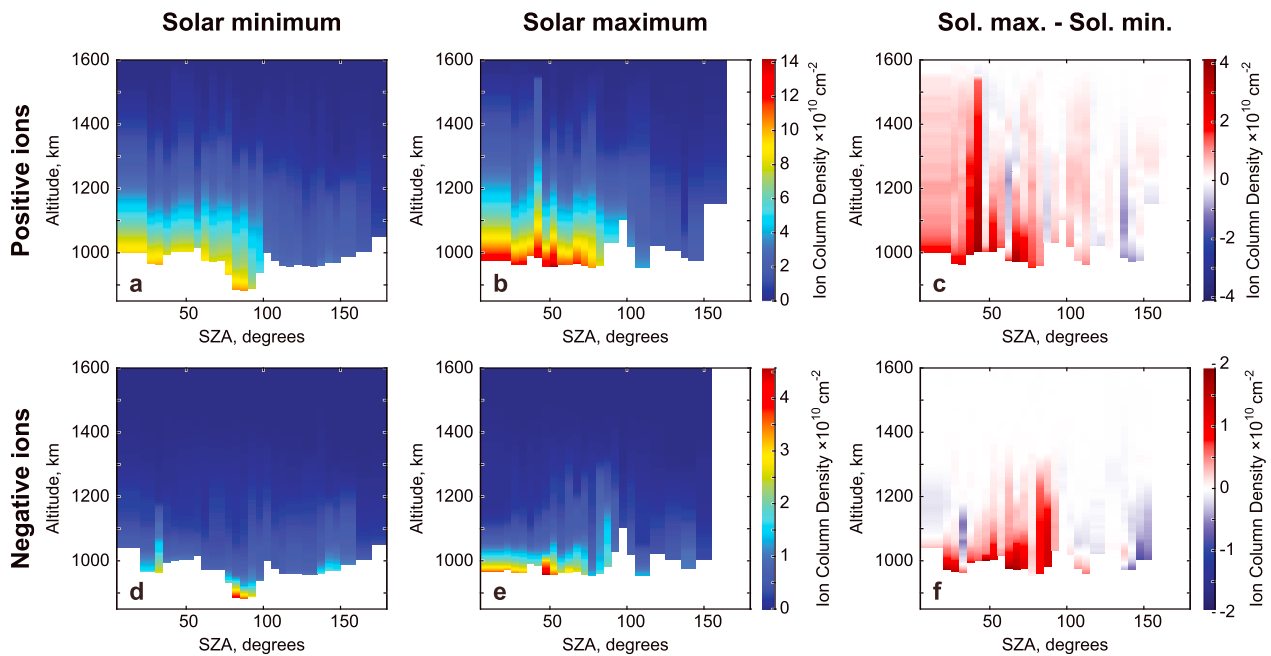


Figure 10. Ion column density, derived from the interpolated (nearest neighbor) RPWS/LP charge densities binned by 5° SZA. (a, d) Solar minimum values, (b, e) solar maximum, and (c, f) the difference between the two. Positive ions are in Figures 10a–10c; negative ions are in Figures 10d–10f. To somewhat equalize the amount of data points between the solar minimum and maximum plots (for interpolation purposes), the EUV limit for sorting has been shifted from 35 to $26.5 \mu\text{W m}^{-2}$.

The increased nightside plasma densities with decreased EUV input on the dayside can also be suspected to be a consequence of a contracted thermosphere, which for a given particle influx would tend to yield a more altitude-concentrated ionospheric peak. Reaction of the thermosphere to the changing EUV flux can be inferred from a corresponding variation of the ion column density profile. The latter may be derived from the RPWS/LP measurements by interpolating the SZA-binned charge densities (Figure 10). The positive ion column density below 1200 km altitude shows an increase of the overall profile (similar across the altitude range) on the dayside, indicating an expansion of the thermosphere. The negative ion column density on the dayside (same altitudes) also increases between the solar minimum and maximum but to a lesser extent. For the nightside, however, both column densities are higher during solar minimum, suggesting that the identified anticorrelation (Figures 6e and 6f) is not an indirect result of an EUV-induced variation in the thermosphere. We plan to investigate this further by invoking neutral number density measurements from the INMS/CSN. It is also noted that the magnetospheric particle influx can vary substantially between individual flybys due to its sensitivity to the magnetic field topology (in addition to variable thermosphere and upstream conditions), which for Titan can be very complicated [e.g., Gronoff *et al.*, 2009; Snowden *et al.*, 2013]. This variability can be investigated with the CAPS/ELS measurements, though these are available only until June 2012, at which time the CAPS instrument was turned off.

4. Conclusions

The solar EUV flux below 80 nm has a strong impact on the ion and dust grain charge densities: a factor ≈ 2 enhancement of the charge densities and a factor ≈ 3 –4 decrease of the nightside charge densities are observed during the solar maximum (as compared to the solar minimum). A plausible scenario for the anticorrelation between the EUV level and the nightside ion densities is an EUV-driven disruption of the chemical production chains and a photodissociation of the heavier long-lived species. During higher solar EUV flux (maximum activity), the altitudes of the peak charge densities decreases for the positive ions and increases for the negative ions/dust grains, the latter reflects the changes of the chemical production of the negative ions/dust grains. Interpretation of this phenomenon requires knowledge of the ion-electron pair production rate which is the aim of our next study. For now we simply conclude that a higher solar EUV flux changes the photochemistry of the upper atmosphere (leading to the observation of less ions on the nightside than at a lower EUV flux) and may then have implications for the aerosol production below the altitudes reachable by the Cassini S/C.

The position of Titan in the Kronian magnetosphere has an unexpected impact on the plasma densities at ~ 1000 km altitude, observed in absence of the ionizing solar radiation (i.e., in the nightside ionosphere), with plasma densities being higher on the sunward side compared to the magnetotail. The specific altitude of these variations is in agreement with the peak ionization by the magnetospheric particle precipitation [Cravens *et al.*, 2008; Galand *et al.*, 2014, Figure 11.25, and references therein]. The magnetotail is typically populated by a larger amount of energetic particles than the sunward magnetosphere and one would expect the trend to be reversed. However, the observations are consistent with the enhancement of the particle flux intensity from the tail toward sunward magnetosphere, detected by the ENA instrument [Mitchell *et al.*, 2009].

Due to the nature of the EUV dependency (power law), no further detrending is sensible with the current data set. This includes investigation of seasons, differences between the A.M. and P.M. regions of the ionosphere, as well as the influence of Saturn's corotational magnetospheric plasma.

The presented observations also strongly imply that the Chapman theory is not applicable for Titan's ionosphere below 1200 km altitude.

References

- Ågren, K., *et al.* (2007), On magnetospheric electron impact ionisation and dynamics in Titan's ram-side and polar ionosphere—a Cassini case study, *Ann. Geophys.*, 25(11), 2359–2369, doi:10.5194/angeo-25-2359-2007.
- Ågren, K., J. E. Wahlund, P. Garnier, R. Modolo, J. Cui, M. Galand, and I. Müller-Wodarg (2009), On the ionospheric structure of Titan, *Planet. Space Sci.*, 57(14–15), 1821–1827, doi:10.1016/j.pss.2009.04.012.
- Ågren, K., N. J. T. Edberg, and J.-E. Wahlund (2012), Detection of negative ions in the deep ionosphere of Titan during the Cassini T70 flyby, *Geophys. Res. Lett.*, 39, L10201, doi:10.1029/2012GL051714.

Acknowledgments

The authors acknowledge funding and RPWS/LP instrument support by the Swedish National Space Board (SNSB) and the Cassini project support by NASA. O.S. acknowledges funding from SNSB, Dnr 130/11:2. E.V. acknowledges funding by the SNSB under contract Dnr 166/14. M.K.G.H. acknowledges the funding from CNRS. N.J.T.E. acknowledges funding by the SNSB under contract Dnr 135/13 and by Vetenskapsrådet under contract 621-2013-4191. K.E.M. acknowledges support from NASA grant NNX13AQ99G. The in situ data used in this paper are included in the figures and listed in the references. The authors thank the TIMED/SEE and SORCE/SOLSTICE instruments' teams for providing the solar irradiance data, available at http://lasp.colorado.edu/lisird/see/level3/3_ssi_ts.html and http://lasp.colorado.edu/lisird/sorce/sorce_ssi/ts.html, respectively.

- Brace, L. H., W. R. Hoegy, and R. F. Theis (1988), Solar EUV measurements at Venus based on photoelectron emission from the Pioneer Venus Langmuir probe, *J. Geophys. Res.*, *93*(A7), 7282, doi:10.1029/JA093iA07p07282.
- Chapman, S. (1931), The absorption and dissociative or ionizing effect of monochromatic radiation in an atmosphere on a rotating earth part II. Grazing incidence, *Proc. Phys. Soc.*, *43*(5), 483–501, doi:10.1088/0959-5309/43/5/302.
- Coates, A. J., F. J. Cray, G. R. Lewis, D. T. Young, J. H. Waite, and E. C. Sittler (2007), Discovery of heavy negative ions in Titan's ionosphere, *Geophys. Res. Lett.*, *34*, L22103, doi:10.1029/2007GL030978.
- Coates, A. J., A. Wellbrock, G. R. Lewis, G. H. Jones, D. T. Young, F. J. Cray, and J. H. Waite (2009), Heavy negative ions in Titan's ionosphere: Altitude and latitude dependence, *Planet. Space Sci.*, *57*(14–15), 1866–1871, doi:10.1016/j.pss.2009.05.009.
- Crary, F. J., B. A. Magee, K. Mandt, J. H. Waite, J. Westlake, and D. T. Young (2009), Heavy ions, temperatures and winds in Titan's ionosphere: Combined Cassini CAPS and INMS observations, *Planet. Space Sci.*, *57*(14–15), 1847–1856, doi:10.1016/j.pss.2009.09.006.
- Cravens, T. E., et al. (2006), Composition of Titan's ionosphere, *Geophys. Res. Lett.*, *33*, L07105, doi:10.1029/2005GL025575.
- Cravens, T. E., I. P. Robertson, S. A. Ledvina, D. Mitchell, S. M. Krimigis, and J. H. Waite (2008), Energetic ion precipitation at Titan, *Geophys. Res. Lett.*, *35*, L03103, doi:10.1029/2007GL032451.
- Cravens T., I. Robertson, J. Waitejr, R. Yelle, V. Vuitton, A. Coates, J. Wahlund, K. Ågren, M. Richard, V. Delahaye (2009), Model-data comparisons for Titan's nightside ionosphere, *Icarus*, *199*(1), 174–188, doi:10.1016/j.icarus.2008.09.005.
- Cui, J., M. Galand, R. V. Yelle, J.-E. Wahlund, K. Ågren, J. H. Waite, and M. K. Dougherty (2010), Ion transport in Titan's upper atmosphere, *J. Geophys. Res.*, *115*, A06314, doi:10.1029/2009JA014563.
- Edberg, N. J. T., J.-E. Wahlund, K. Ågren, M. W. Morooka, R. Modolo, C. Bertucci, and M. K. Dougherty (2010), Electron density and temperature measurements in the cold plasma environment of Titan: Implications for atmospheric escape, *Geophys. Res. Lett.*, *37*, L20105, doi:10.1029/2010GL044544.
- Edberg, N. J. T., D. J. Andrews, O. Shebanits, K. Ågren, J.-E. Wahlund, H. J. Opgenoorth, T. E. Cravens, and Z. Girazian (2013), Solar cycle modulation of Titan's ionosphere, *J. Geophys. Res. Space Physics*, *118*, 5255–5264, doi:10.1002/jgra.50463.
- Galand, M., R. Yelle, J. Cui, J.-E. Wahlund, V. Vuitton, A. Wellbrock, and A. J. Coates (2010), Ionization sources in Titan's deep ionosphere, *J. Geophys. Res.*, *115*, A07312, doi:10.1029/2009JA015100.
- Galand, M., A. J. Coates, T. E. Cravens, and J.-E. Wahlund (2014), Titan's ionosphere, in *Titan*, edited by I. Müller-Wodarg, C. A. Griffith, E. Lellouch, and T. E. Cravens, pp. 376–418, Cambridge Univ. Press, Cambridge.
- Gronoff, G., J. Liliensten, and R. Modolo (2009), Ionization processes in the atmosphere of Titan, *Astron. Astrophys.*, *506*(2), 965–970, doi:10.1051/0004-6361/200912125.
- Gurnett, D. A., et al. (2004), The Cassini radio and plasma Wave investigation, *Space Sci. Rev.*, *114*(1–4), 395–463, doi:10.1007/s11214-004-1434-0.
- Holmberg, M. K. G., J.-E. Wahlund, M. W. Morooka, and A. M. Persoon (2012), Ion densities and velocities in the inner plasma torus of Saturn, *Planet. Space Sci.*, *73*(1), 151–160, doi:10.1016/j.pss.2012.09.016.
- Jacobsen, K. S., J.-E. Wahlund, and A. Pedersen (2009), Cassini Langmuir probe measurements in the inner magnetosphere of Saturn, *Planet. Space Sci.*, *57*(1), 48–52, doi:10.1016/j.pss.2008.10.012.
- Lavvas, P., et al. (2013), Aerosol growth in Titan's ionosphere, *Proc. Natl. Acad. Sci.*, *110*(8), 2729–2734, doi:10.1073/pnas.1217059110.
- Madanian, H., T. E. Cravens, M. S. Richard, J. H. Waite, N. J. T. Edberg, J. H. Westlake, and J.-E. Wahlund (2016), Solar cycle variations in ion composition in the dayside ionosphere of Titan, *J. Geophys. Res. Space Physics*, *121*, 8013–8037, doi:10.1002/2015JA022274.
- Mitchell, D. G., et al. (2009), Recurrent energization of plasma in the midnight-to-dawn quadrant of Saturn's magnetosphere, and its relationship to auroral UV and radio emissions, *Planet. Space Sci.*, *57*(14–15), 1732–1742, doi:10.1016/j.pss.2009.04.002.
- Müller-Wodarg, I. C. F., R. V. Yelle, J. Cui, and J. H. Waite (2008), Horizontal structures and dynamics of Titan's thermosphere, *J. Geophys. Res.*, *113*, E10005, doi:10.1029/2007JE003033.
- Niemann, H. B., et al. (2005), The abundances of constituents of Titan's atmosphere from the GCMS instrument on the Huygens probe, *Nature*, *438*(7069), 779–784, doi:10.1038/nature04122.
- Rosenqvist, L., J. E. Wahlund, K. Ågren, R. Modolo, H. J. Opgenoorth, D. Strobel, I. Müller-Wodarg, P. Garnier, and C. Bertucci (2009), Titan ionospheric conductivities from Cassini measurements, *Planet. Space Sci.*, *57*(14–15), 1828–1833, doi:10.1016/j.pss.2009.01.007.
- Sagnières, L. B. M., M. Galand, J. Cui, P. P. Lavvas, E. Vigren, V. Vuitton, R. V. Yelle, A. Wellbrock, and A. J. Coates (2015), Influence of local ionization on ionospheric densities in Titan's upper atmosphere, *J. Geophys. Res. Space Physics*, *120*, 5899–5921, doi:10.1002/2014JA020890.
- Schunk, R., and A. Nagy (2009), *Ionospheres*, 2nd ed., pp. 260–264, Cambridge Univ. Press, Cambridge.
- Shebanits, O., J.-E. Wahlund, K. Mandt, K. Ågren, N. J. T. Edberg, and J. H. Waite (2013), Negative ion densities in the ionosphere of Titan—Cassini RPWS/LP results, *Planet. Space Sci.*, *84*, 153–162, doi:10.1016/j.pss.2013.05.021.
- Shebanits, O., et al. (2016), Ion and aerosol precursor densities in Titan's ionosphere: A multi-instrument case study, *J. Geophys. Res. Space Physics*, *121*, 10,075–10,090, doi:10.1002/2016JA022980.
- Snowden, D., R. V. Yelle, M. Galand, A. J. Coates, A. Wellbrock, G. H. Jones, and P. Lavvas (2013), Auroral electron precipitation and flux tube erosion in Titan's upper atmosphere, *Icarus*, *226*(1), 186–204, doi:10.1016/j.icarus.2013.05.021.
- Thissen, R., O. Witasse, O. Dutuit, C. S. Wedlund, G. Gronoff, and J. Liliensten (2011), Doubly-charged ions in the planetary ionospheres: A review, *Phys. Chem. Chem. Phys.*, *13*(41), 18264, doi:10.1039/c1cp21957j.
- Vigren, E., et al. (2013), On the thermal electron balance in Titan's sunlit upper atmosphere, *Icarus*, *223*(1), 234–251, doi:10.1016/j.icarus.2012.12.010.
- Vigren, E., M. Galand, O. Shebanits, J.-E. Wahlund, W. D. Geppert, P. Lavvas, V. Vuitton, and R. V. Yelle (2014), Increasing positive ion number densities below the peak of ion-electron pair production in Titan's ionosphere, *Astrophys. J.*, *786*(1), 69, doi:10.1088/0004-637X/786/1/69.
- Vigren, E., et al. (2015), Ionization balance in Titan's nightside ionosphere, *Icarus*, *248*, 539–546, doi:10.1016/j.icarus.2014.11.012.
- Vuitton, V., O. Dutuit, M. A. Smith, and N. Balucani (2014), Chemistry of Titan's atmosphere, in *Titan*, edited by I. Müller-Wodarg, C. A. Griffith, E. Lellouch, and T. E. Cravens, pp. 224–284, Cambridge Univ. Press, Cambridge.
- Wahlund, J.-E. (2005), Cassini measurements of cold plasma in the ionosphere of Titan, *Science*, *308*(5724), 986–989, doi:10.1126/science.1109807.
- Wahlund, J.-E., et al. (2009), Detection of dusty plasma near the E-ring of Saturn, *Planet. Space Sci.*, *57*(14–15), 1795–1806, doi:10.1016/j.pss.2009.03.011.
- Wellbrock, A., A. J. Coates, G. H. Jones, G. R. Lewis, and J. H. Waite (2013), Cassini CAPS-ELS observations of negative ions in Titan's ionosphere: Trends of density with altitude, *Geophys. Res. Lett.*, *40*, 4481–4485, doi:10.1002/grl.50751.
- Westlake, J. H., J. M. Bell, J. H. Waite, R. E. Johnson, J. G. Luhmann, K. E. Mandt, B. A. Magee, and A. M. Rymer (2011), Titan's thermospheric response to various plasma environments, *J. Geophys. Res.*, *116*, A03318, doi:10.1029/2010JA016251.